Alternative first-principles calculation of entropy for liquids

Edmund R. Meyer, Christopher Ticknor, Joel D. Kress, and Lee A. Collins

Phys. Rev. E **93**, 042119 — Published 15 April 2016

DOI: 10.1103/PhysRevE.93.042119

Alternative first principles calculation of entropy for liquids

Edmund R. Meyer,* Christopher Ticknor, Joel D. Kress, and Lee A. Collins
Theoretical Division, Los Alamos National Laboratory, Los Alamos, New Mexico 87545, USA
(Dated: March 24, 2016)

We present an alternative method for interpreting the velocity auto-correlation function (VACF) of a fluid with application to extracting the entropy in a manner similar to the methods developed by Lin *et al.* [J. Chem Phys. **119**, 11792 (2003)] and improved upon by Desjarlais [Phys. Rev. E **88**, 062145 (2013)]. The liquid VACF is decomposed into two components, one gas and one solid, and each contribution's entropic portion is calculated. However, we fit *both* the gas and solid portions of the VACF in the time domain. This approach is applied to a single-component liquid (a two-phase model of liquid Al at the melt line) and two different two-component systems: a superionic-to-superionic (BCC to FCC) phase transition in H_2O at high temperatures an pressures and a metastable liquid state of MgO. For all three examples, comparisons to existing results in the literature demonstrate the validity of our alternative.

PACS numbers: 02.70.-c,65.20.-w

I. INTRODUCTION

In order to describe the phase diagram of liquids it is essential to know the entropy and free energy. Calculating these quantities from first principles for liquid systems remains a challenge. Even in molecular dynamics (MD), which implicitly accounts for entropy, directly calculating entropy remains elusive. A myriad of approaches to the problem have been considered. Thermodynamic integration[1–5] is a preferred method for calculating entropies, but it comes at great computational cost due to the many *ab initio* simulations one must perform shifting from the actual simulation to the reference system with known properties. In addition, one needs a good reference system otherwise there could be too many integration points along the thermodynamic integration path.

Several methods have been developed to treat explicitly the conditions around melt such as two-phases [6–10], the Z-method [11–14], and the heat-until-it-melts (HUM) and hysterisis methods [15, 16], approaches that proceed by directly categorizing the phases of constiuents in MD simulations. By monitoring the relative populations of the two phases - liquid and solid - as simulation parameters are varied, the melt line can be mapped. While these methods yield valuable and important results, some are computationally expensive while others are susceptible to metastablity and relatively larger errors. We seek a more general formulation that perfoms over a broader range of liquid conditions.

Such a new, computationally efficient two-phase thermodynamic (2PT) method for calculating entropy is that of Lin *et al*[17, 18]. Only the primary MD simulation is used to compute the entropy and free energy. Entropy is obtained by decomposing the velocity auto-correlation function (VACF), and the related vibrational density of states, into solid- and gas-like subsystems. The original formulation of Lin *et al.* was developed and used with Lennard-Jones potentials[18–20]. However, when applied to liquid metals the result was over-estimated[21] (a few percent compared to experiment) thus requiring the introduction of the memory function approach of Desjarlais[22].

With the improved 2PT memory function (2PT-MF) model [22] for calculating entropies for liquid systems, molecular dynamics (MD) calculations are being pushed with vigor to studying systems near liquid-solid phase boundaries [23]. As mentioned, the approach relies on calculating the VACF of the system, which tells us about the "phonon" density of states in the liquid. We use the term "phonon" loosely here since the method relies on separating the liquid into a gas-like and a solid-like portion. It is the solid-like portion with which we would associate any phonon-like modes. However, we cannot discount structure which might form in the gaseous state.

Comparisons between methods like thermodynamic integration [1–4] and 2PT-MF were done in Ref. [22] for liquid Na and Al. Application to the melt curve of Al at 4000 K was performed in Ref. [23]. The key characteristic is that the entropy can be calculated directly from the molecular dynamics simulation without the need of some intermediate integration step. Therefore, knowing the energy, pressure, volume, and entropy of two systems from the corresponding MD simulation allows one to make comparable estimates of which system has the lower Gibb's free energy and is therefore thermodynamically more stable. This saves considerable computational cost.

*Electronic address: meyere@lanl.gov

The location of melting curves goes well beyond liquid metals, being important to planetary science [24], inertial confinement fusion [25], and other condensed/soft matter applications. When confronted with the daunting task of a large pressure-temperature space to explore, and many phases to consider, a computationally efficient method to determine the entropy, such as the 2PT-MF method of Desjarlais, is a must. The 2PT method in its simplest form [17, 18] is a unique step in approaching the problem of extracting thermodynamic properties from MD-derived VACFs, which lead to a vibrational density of states. The 2PT method considers the fluid nature of the system, especially the effects at low frequency, together with quantum corrections to the ionic motion in order to extract the desired thermodynamic information. The 2PT-MF method [22] goes further by providing a more rigorous algorithm, using the Gaussian ansatz for the memory function of the gas portion of the VACF, which preserves sum rules and corrects the the high frequency behavior of the hard-sphere model used in the 2PT method. This leads to better accuracies for softer inter-atomic potentials.

However, the model attributes all structure in the VACF to the solid-like portion by assuming that the gas-like portion satisfies a Gaussian ansatz. In both 2PT and 2PT-MF, the remainder of the non-fitted gas-portion must be due to the solid and is treated numerically, which leaves a gap in understanding within the models for what the solid portion is contributing. Yet, a real gas can and does have structure that should be taken into account. Additionally, having a model for the form that the solid portion takes will alleviate the high frequency noise associated with the tail of the Fourier transform of the VACF; this can be due to the time step in the MD simulation, length of MD trajectory as well as numerical noise. In the method we develop in this paper, we use an analytic formulation for the solid portion of the VACF which allows us to perform the Fourier transform against a weighting function smoothly without the associated noise of numerical integration. In addition, our model is constructed so as to satisfy sum rules up to third-order guaranteeing at least a $1/\omega^6$ decay in the high-frequency spectrum.

In what follows we will present an alternative derivation of the 2PT-MF model using a memory function approach based on the itinerant oscillator model [26]. This gives a natural breakdown of the VACF into two components, a gas-like contribution which contains the diffusive nature of the system, and a solid-like contribution, which contains the phonon-like nature of the system. We first derive the VACF in Sec. II and then walk through examples from the literature as a test of the method. In Sec. IV we examine the Al melt curve at 4000 K as in Ref. [23], the difference in states of superionic water for various P and T as in Ref. [27], and MgO at 10000 K for various P as in Ref. [28]. We then conclude and give areas for future consideration.

II. MEMORY FUNCTION

Our starting point will be the itinerant oscillator model of Sears [26] as expanded upon by Damle, Sjölander, and Singwi [29]. The basic concept is that there is a particle of interest, denoted with the subscript 0 connected to a bath denoted with a subscript 1. Through a basic stochastic set of equations as outlined in Refs. [26, 29, 30], one arrives at a memory function (MF) that the velocity auto-correlation function (VACF) of the particle of interest must obey. This MF is given by

$$\tilde{K}(p) = \mu_0(p) + \frac{\lambda_{01}^2(p + \tilde{\mu}_1(p))}{p(p + \tilde{\mu}_1(p)) + \lambda_{10}^2}, \tag{1}$$

where the $\sim$ represents that this function is in Laplace space. The coupling parameters λ_{01} and λ_{10} are how the particle of interest couples to the bath and are related to each other by the fluctuation-dissipation theorem and Newton's third law[29]. The two terms $\tilde{\mu}_0(p)$ and $\tilde{\mu}_1(p)$ describe how the free particle and medium "remember" their histories, i.e. they are friction terms in the stochastic oscillator equations.

From the MF, we obtain the VACF in Laplace space as

$$\frac{\tilde{\phi}(p)}{\phi_{00}} = \frac{1}{p + \tilde{K}(p)}, \tag{2}$$

with ϕ_{00} the overall scale of the VACF which is given by the zero time value, $3\,k_B\,T/M_0$, where M_0 is the mass of the particle of interest.

The zero-frequency limit of $\tilde{\phi}(p)$ is related to the diffusion of the particle. By taking the $p \to 0$ limit of Eq. (2) using the form of Eq. (1) we arrive at

$$\tilde{\mu}_0(0) + \frac{\lambda_{01}^2}{\lambda_{10}^2}\tilde{\mu}_1(0) = \frac{k_B T}{M_0 D}, \tag{3}$$

where D is the diffusion coefficient. Eq. (3) gives us a hint as to what forms $\tilde{\mu}_0(p)$ and $\tilde{\mu}_1(p)$ should take. The MF nicely separates into two pieces, and the low frequency limit does as well. We want to associate $\tilde{\mu}_0(p)$ with the gas-like

diffusion of the system and $\tilde{\mu}_1(p)$ with the solid-like behavior. This means that any choice of the auto-correlation function (ACF) must have $\tilde{\mu}_1(0) = 0$. A natural choice is a cosine, which is a traditional choice for a solid.

Additionally, there is a high frequency limit which we can find by taking the $p \to \infty$ limit. Matching powers of the Laplace transform of the moment expansion of the VACF we find that

$$\lim_{p\to\infty} \langle \omega^2 \rangle = p\,\tilde{\mu}_0(p) + \lambda_{01}^2. \tag{4}$$

The second moment of the power spectrum will be given by the gas term and by the constraints on the parameter λ_{01}^2. This parameter will be fit in the end, but is related to the solid. So the high frequency limit has contributions from both the solid- and gas-like components in this model.

A key tenant of the two-phase thermodynamic model (2PT) is that the VACF can be split into two components, a gas and a solid portion. In the itinerant oscillator model, so far, that cannot be done since it is the MF which naturally separates into gas and solid portions. However, in the limit that the coupling of the particle to the medium is small, $\lambda_{01} \ll 1$, we can expand Eq. (2) to find

$$\frac{\tilde{\phi}(p)}{\phi_{00}} = \frac{1}{p+\tilde{\mu}_0(p)} - \frac{\lambda_{01}^2}{(p+\tilde{\mu}_0(p))^2}\frac{p+\tilde{\mu}_1(p)}{p(p+\tilde{\mu}_1(p)) + \lambda_{10}^2}, \tag{5}$$

$$= \frac{\tilde{\phi}_{\rm gas}(p)}{\phi_{00}} + \frac{\tilde{\phi}_{\rm solid}(p)}{\phi_{00}} \tag{6}$$

What remains is to choose a form of the friction term $\tilde{\mu}_0(p)$ as well as to take the inverse Laplace transform of the equation to get the VACF in real space.

An exponential is a typical choice for the ACF that leads to $\tilde{\mu}_0(p)$, it in turn leads to a violation of the first moment relation, i.e. the first derivative of the VACF with respect to time will not be zero at $t = 0$. Once can use the continued fraction approach for $\tilde{\mu}_0(p)$ and the Laplace, but the inverse Laplace transforms become untenable beyond a two levels. Using the second continued fraction for the ACF of $\mu_0(t)$ and a cosine for $\mu_1(t)$ leads in Laplace space to

$$\tilde{\mu}_0(p) = \frac{a^2}{p + \frac{b_1^2}{p+\frac{b_2^2}{p+\delta}}}, \tag{7}$$

$$\tilde{\mu}_1(p) = \frac{c^2 p}{p^2+\eta^2}, \tag{8}$$

and generates tractable solutions for both the gas and solid portions. While not trivial, the inverse Laplace transforms of Eqs. (7) and (8), when inserted into Eq. (5) can be taken. We make substitutions to bring the polynomials into regular forms for inverting Laplace transforms. Then some minor algebraic manipulation of the gas portion and major manipulation of the solid portion leads to

$$\frac{\phi_{\rm gas}(t)}{\phi_{00}} = f_{\rm gas}\left(\frac{\gamma_2(\gamma_2^2+\varphi^2)}{(\gamma_1+\gamma_2)((\gamma_2-2\gamma_1)^2+4\varphi^2)}e^{-\gamma_1 t}\right. \tag{9}$$
$$\left. + e^{-\gamma_2 t/2}\left(\frac{\gamma_1}{\gamma_1+\gamma_2}\frac{4(\varphi^2+\gamma_1^2)-3\gamma_2^2}{4\varphi^2+(\gamma_2-2\gamma_1)^2}\cos(\varphi t) + \frac{\gamma_1\gamma_2}{2\varphi(\gamma_1+\gamma_2)}\frac{12\varphi^2+4\gamma_1^2-\gamma_2^2}{4\varphi^2+(\gamma_2-2\gamma_1)^2}\sin(\varphi t)\right)\right),$$

$$\frac{\phi_{\rm solid}(t)}{\phi_{00}} = f_{\rm solid}\left(\frac{1}{1-\frac{\beta}{\sqrt{\beta^2+\eta^2}}}e^{-\beta t}(1-\beta t) - \frac{\beta(\beta+\sqrt{\beta^2+\eta^2})}{\eta^2}e^{-\sqrt{\beta^2+\eta^2}t}\left(\cos(\eta t) - \frac{\sqrt{\beta^2+\eta^2}}{\eta}\sin(\eta t)\right)\right) \tag{10}$$

The time constants β, γ_1, and γ_2, vibratory constants φ and η as well as constants $f_{\rm gas}$ and $f_{\rm solid}$ are all fit parameters, but they can be related back to the parameters in the itinerant oscillator model contained in Eqs. (5), (7), and (8). The terms $f_{\rm gas}$ and $f_{\rm solid}$ are related. The numerical prefactors in front of the exponentials and sines and cosines are chosen in a very specific manner such that $\int_0^\infty F_{\rm gas}(\nu)d\nu = 3$, due to the number of degrees of freedom, and $F_{\rm gas}(\nu) = (1/f_{\rm gas})\int_0^\infty \phi_{\rm gas}(t)\cos(2\pi\nu t)dt$. The same is true for $F_{\rm solid}$. In addition, both the gas and solid portions satisfy the first and third derivative of the VACF being zero at $t = 0$ ensuring at least a $1/\omega^6$ decay in the frequency spectrum at high frequencies. With the requirement that

$$\frac{\phi_{\rm total}(0)}{\phi_{00}} = \frac{\phi_{\rm solid}(0)}{\phi_{00}} + \frac{\phi_{\rm gas}(0)}{\phi_{00}} = 1, \tag{11}$$

we get that $f_{\rm solid} = 1 - f_{\rm gas}$. With these normalizations the factors $f_{\rm gas}$ and $f_{\rm solid}$ act like gas and solid fractions.

In deriving Eq. (10) we made an approximation to ignore the oscillating terms which did not have exponential dampening. While in principle these terms could be extracted from a fit to a VACF, the numerical noise is usually too great, and we therefore chose to exclude them from the model. Additionally, we allow the time scale in the solid to vary freely from that in the gas even though they should be related. This was a consequence of requiring each component to individually satisfy the derivative rules.

Solving Eq. (3) for D yields

$$D = f_{\rm gas}\frac{k_B T}{M_0}\gamma_2\left(\frac{1}{\gamma_1^2+\gamma_1\gamma_2}+\frac{4}{\gamma_2^2+4\varphi^2}\right). \tag{12}$$

As the gas fraction diminishes so too does the diffusion constant. Additionally, as the vibratory timescale, φ, becomes longer than the exponential timescale with which it moves through the medium,γ_2, the amount that this term contributes to diffusion also tends to zero. Upon solving Eq. (4), the second moment is given by

$$\langle\omega^2\rangle = f_{\rm gas}\frac{\gamma_1}{\gamma_1+\gamma_2}\frac{\gamma_2+4\varphi^2}{4}+f_{\rm solid}\beta\left(2\sqrt{\beta^2+\eta^2}-\beta\right), \tag{13}$$

which clearly has the gas and solid terms as expected.

III. TWO PHASE THERMODYNAMIC MODEL

The 2PT model as developed in Refs. [17, 18] and expanded to use the MF in Ref. [22] (referred to as the 2PT-MF model) has been used to calculate entropy of liquids near melt curves with some degree of accuracy (10-20%) [23]. The key tenant of the model is that the VACF of a liquid can be broken down into a gas and solid set of components and then separately integrated against their respective weighting functions and summed to get the total entropy.

In the 2PT-MF model, the gas fraction $f_{\rm gas}$ is a fitting parameter as in our model, but the model assumes a very simple form (a Gaussian) for the gas-like portion. This does not allow for the gas to have any structure and therefore relies on averaging through oscillations when fitting with the Gaussian. In the present model, structure in the gas is accounted for by the vibratory terms seen in Eq. (9). Additionally, unlike the 2PT-MF model, there is a prediction for the form of the solid piece as given by Eq. (10).

The details of the 2PT-MF method are well outlined in Refs. [22, 23] and therefore only the pertinent changes are given here. The gas-like fraction starts with the assumptions of hard spheres. A good starting point is the Carnahan-Starling equation of state[31]. This takes the excess entropy for a hard sphere fluid from the packing fraction χ. In the 2PT-MF model, we must solve the hard sphere packing fraction [17]

$$\frac{2(1-\chi)^3}{2-\chi}-\chi^{2/5}\Delta^{3/5}=0, \tag{14}$$

where

$$\Delta = \frac{8}{3}\left(\frac{6}{\pi}\right)^{2/3} D\sqrt{\frac{\pi M_0}{k_B T}}\left(\frac{N}{V}\right)^{1/3}, \tag{15}$$

and D is given by Eq. (12). (By construction the solid-contribution to the diffusion constant is identically zero.) Once we have χ we know the entropy from the gas contribution

$$S_{\rm gas} = 3\,N\,k_B f_{\rm gas} W_{\rm gas}, \tag{16}$$

where $W_{\rm gas}$ is the sum of the Sackur-Tetrode ideal gas and excess

$$\begin{aligned} W_{\rm gas} &= W_{\rm IG} + W_{\rm x}, \\ 3\,W_{\rm IG} &= \frac{5}{2}+\ln\left[\left(\frac{M_0 k_B T}{2\pi\hbar^2}\right)^{3/2}\frac{V}{f_{\rm gas}N}\right], \qquad (17)\\ 3\,W_{\rm x} &= \ln\left[\frac{1+\chi+\chi^2-\chi^3}{(1-\chi)^3}\right]+\frac{\chi(3\chi-4)}{(1-\chi)^2}. \qquad (18) \end{aligned}$$

Next we evaluate the solid portion. In the traditional 2PT-MF, one would subtract from the numerical VACF the Gaussian fit obtained by matching the low and high frequency constraints. Here, we have already obtained a form

for the solid portion of the VACF, and there is thus no need for numerical integration. The solid contribution to the entropy is then given by

$$S_{\rm solid} = N\,k_B f_{\rm solid} \int_0^\infty F_{\rm solid}(\nu) W_{\rm solid}(\nu) d\,\nu, \tag{19}$$

with $F_{\rm solid}$ the Fourier transform of $\phi_{\rm solid}(t)$ and $W_{\rm solid}(\nu)$ the harmonic weighting function [32]. The total entropy for the liquid is then

$$S_{\rm liquid} = S_{\rm solid} + S_{\rm gas} \tag{20}$$

We can fit the VACF from the MD simulations to the combined forms in Eqs. (9) and (10) in terms of our fitting parameters, and we can now calculate the entropy of a liquid by fitting the VACF in the time-domain. This has the advantage that we know the long-time behavior of the VACF, as it must approach zero. The fits will be dominated by the structure that appears in the early-time behavior of the VACF. The late-time behavior takes the longest to converge in a MD simulation and with this approach we are able to reduce the number of time steps needed, even more so than is already done in the 2PT-MF method [23] because we don't need as small a time step to resolve the high-frequency behavior.

IV. APPLICATIONS

We test our version of the 2PT-MF approach by comparing with calculations on Aluminum [23] that use the original formulation[22]. In addition, we apply the method to water in two phases [27] and to MgO [28]. The application to water involves a superionic mixture, in which the hydrogen are mobile and the oxygen are in a solid lattice. Thus we integrate the whole oxygen VACF against the harmonic weighting function. Finally, MgO at 10000 K between 200 GPa and 400 GPa has both components in a meta-stable liquid-like state.

For all calculations, we use the Vienna *ab initio* Simulation Package, (VASP) [33–36], version 5.2.12. The electronic wave-function is determined from Finite-Temperature Density Functional Theory within the Kohn-Sham convention [37–42]. Projector-augmented wave (PAW) pseudo-potentials [43, 44] are used to model the electron-ion interaction in addition to the exchange-correlation functional of Perdew, Burke, and Ernzerhof [45] (GGA). The electron temperature, in local thermodynamic equilibrium with the ions, was introduced through the Mermin[39] prescription and set by a Fermi-Dirac weighting of the occupied bands[41].

A. Aluminum

In Ref. [23] the authors analyzed Aluminum along the FCC melt curve at $T = 4000$ K, which we aim to reproduce using this complete VACF fitting method. We used 108 Al atoms starting in the FCC geometry at densities of 3.0, 3.2, 3.6, 4.0, and 4.4 g/cm^3. We employed the PAW pseudopotential that contains 3 valence electrons for Al with a fixed cutoff energy of 300 eV. We applied velocity scaling at each step to fix the temperature to 4000 K. Our time step was 1 fs, in accordance with the convergence test performed in Ref. [23].

In Fig. 1 we plot the VACF for the $\rho = 3.0$ g/cm^3 at $T = 4000$ K for Al. In the top panel, we present both the results from the VASP simulation and the fit using Eqs. (9) and (10). As is evident, the fit captures well the essential structural features of the VACF, reproducing the first minimum and maximum.

Additionally, we can separate the VACF into the constituent parts (middle panel Fig. 1). The gas portion is seen to be the dominant part and also captures a large portion of the vibratory pattern. Physically, one can think of the vibratory pattern as hindered diffusion of the particle due to the medium. The solid portion encapsulates how much of that hindrance is actually more of a permanence.

In the bottom panel of Fig. 1, we plot the power spectrum (Fourier transform) of each component. As expected the gas component gives the zero frequency value, and the solid component rapidly approaches zero at zero frequency playing no part in diffusion. However, both the solid and gas components play a part in the high frequency behavior of the tail of the VACF as constructed in this model, as both fall off with a $1/\omega^6$ tail by construction.

The general fitting procedure requires an MD simulation for a trajectory long enough to converged the VACF. First we take an initial Fourier transform of the data and look for frequencies in the signal which will give possible starting guesses for φ and η. Good starting guesses for γ_1 and γ_2 can be obtained from the $1/e$ time of the VACF. If oscillations are not strong about the time axis, $f_{\rm gas}$ is likely larger than $f_{\rm solid}$. As oscillations get stronger, i.e., cross the axis multiple times, larger values for $f_{\rm solid}$ become more appropriate. A standard non-linear fitting routine such as Levenberg-Marquardt or Conjugate-Gradient will suffice for finding the optimum parameters. We apply a

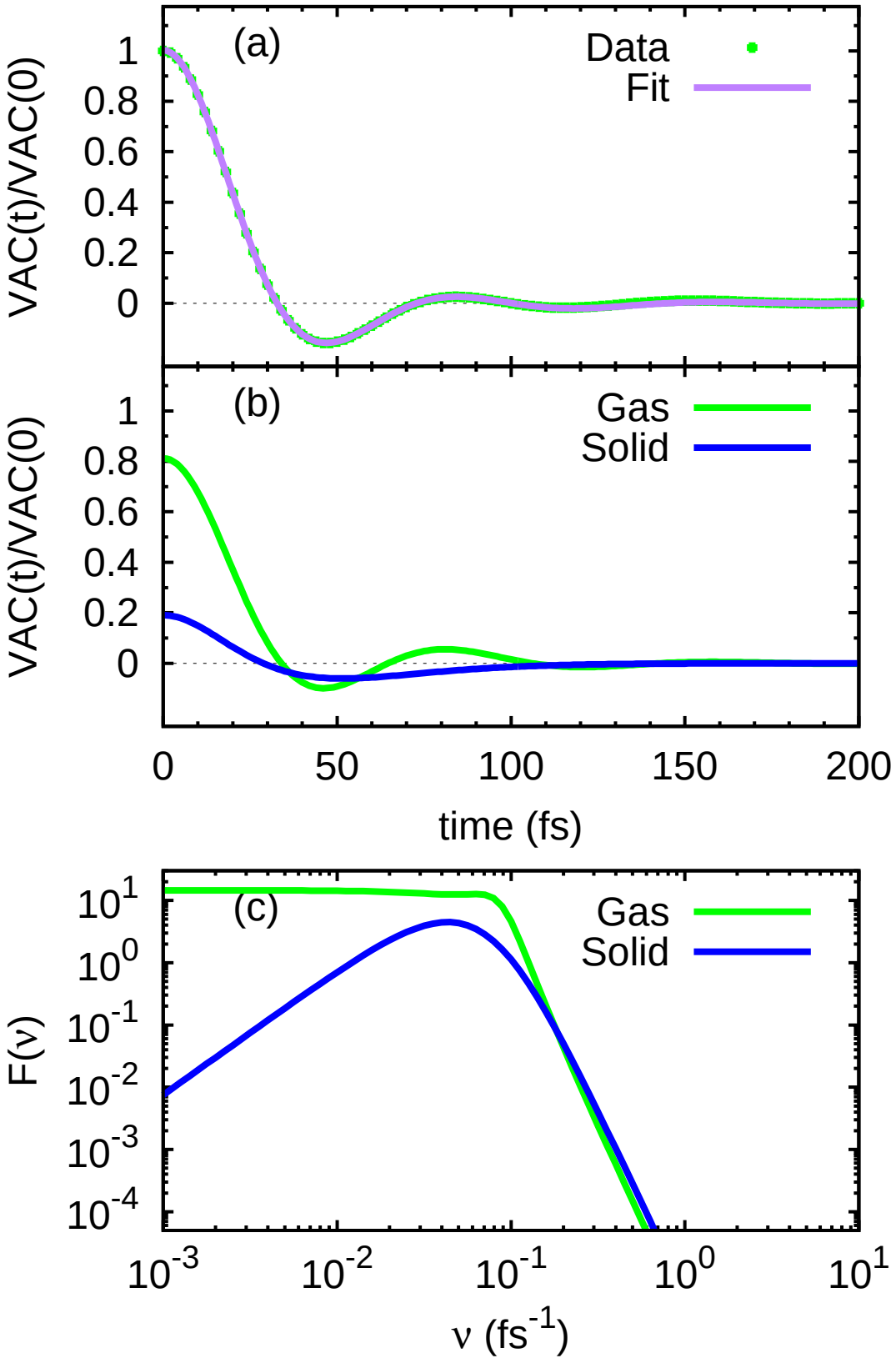

FIG. 1: (color online) Al at $T = 4000\,\mathrm{K}$ and $\rho = 3.0\,\mathrm{g/cm^3}$. Top panel is the raw QMD data (green plus) and the fit (solid line) which is the sum of Eqs. (9) and (10). Middle panel are the individual contributions to the VACF: gas (green solid line) and solid (blue dashed line). Bottom panel is the power spectrum for both the gas (green solid line) and solid (blue dashed line).

weight function of $exp(-t/\tau_{\rm window})$, where $\tau_{\rm window}$ is the window over which we collected data on the VACF, necessary because the early-time portion of the VACF is better converged than the late-time portion of the VACF. We tried other forms of the weight function such as $exp(-t/2\tau_{\rm window})$ and $exp(-2t/\tau_{\rm window})$ with little change in the result.

$f_{\rm gas}$	(Constant)	0.79(6)
γ_1	($\rm fs^{-1}$)	$4.49(6) \times 10^{-2}$
γ_2	($\rm fs^{-1}$)	$5.64(3) \times 10^{-2}$
φ	($\rm fs^{-1}$)	$8.286(5) \times 10^{-2}$
$f_{\rm solid}$	(Constant)	0.21(6)
β	($\rm fs^{-1}$)	$6.24(4) \times 10^{-2}$
η	($\rm fs^{-1}$)	$3.85(7) \times 10^{-2}$

TABLE I: Fit parameters for the case of Al at $T = 4000\,\rm K$ and $\rho = 3.0\,\rm g/cm^3$. All values are in units of $\rm fs^{-1}$ except $f_{\rm gas}$ and $f_{\rm solid}$ which are unitless. The number in parentheses is the standardized fit error in the last digit. The overall adjusted-R^2 value is 0.999914.

In Table I, we give the results of the fitting procedure for the case presented in Fig. 1 of Al at $T = 4000\,\rm K$ and $\rho = 3.0\,\rm g/cm^3$. The model produces a very good fit with an adjusted-R^2 near unity. The sum of $f_{\rm gas}$ and $f_{\rm solid}$ is unity as expected, but was not enforced in the fit.

We now apply this fitting procedure to the remaining densities in Table II. Our entropies agree well with those of Ref. [23] given that both results are expected to be accurate to the 10-20% level. We only compare our model to that of the liquid results under the assumption that the coupling between the particle of interest and medium is small. With the onset of solidification, or in the case of an actual solid, it is not clear that this assumption is valid.

ρ ($\rm g/cm^3$)	S (This Work) (kJ/K/kg)	S (Ref. [23]) (kJ/K/kg)
3.0	3.73	3.55
3.2	3.42	3.44
3.6	3.17	3.25
4.0	2.79	3.08
4.4	2.50	2.94

TABLE II: Entropic results S for the liquid phase along the melt curve at $T = 4000\,\rm K$ of Al for density ρ. Comparison between the present method and the 2PT-MF presented in Ref. [23].

In the case of the solid-side of the melt curve, we can take the numerical cosine transform and then integrate the result against the solid weighting function to extract the entropy. We obtain 2.92 and 2.80 kJ/K/kg, at 4.0 and $4.4\,\rm g/cm^3$, respectively, for the solid-side of the melt-curve of Al; this compares favorably to the values 2.86 and 2.73 kJ/K/kg found in Ref. [23]. Using our fitting model to extract the gas-like and solid-like fractions, we get small values for $f_{\rm gas}$ as expected which in turn leads to small values of the diffusion coefficient D. However, small, but non-zero, values of D and $f_{\rm gas}$ can lead to large, varying terms for $S_{\rm gas}$ via Eqs. (16), (17), and (18). Therefore, in situations where D is known, or at least expected to be zero, we find it prudent to treat the system purely as a solid.

B. Water

Recently Wilson, Wong, and Militzer [27] studied a superionic to superionic (BCC to FCC) phase transition of water at several pressures and temperatures, where the O atoms form a lattice and the H atoms diffuse freely. We aim to reproduce some of those results as a proof of principle of this method. In order to calculate the entropy of the mixture, one must compute the VACF for each component of the system; in this case the H and O atoms. Our aim is to compare the entropies between the BCC and FCC phases at 100 GPa and 3000 K; 1000 GPa and 5000 K; and 4000 GPa and 5000 K.

The convergence tests in Ref. [27] suggest using a 2x2x2 Γ-centered k-point grid and a cubic cell. We optimized each cell in each phase so that the pressures matched to within $\lesssim 1\%$ and then run each simulation for 8000 (12000) steps in the BCC (FCC) phases. The BCC (FCC) used 54 (32) molecules. Additionally we used a 0.25 fs (0.2 fs) time step at 3000 K (5000 K) in accordance with the work in Ref. [27].

	P (GPa)	T (K)	ΔG (eV/mol)	ΔU (eV/mol)	PΔV (eV/mol)	-TΔS (eV/mol)
Present	100	3000	0.071	0.0039	0.016	0.051
[27]			0.002(11)	-0.037(20)	0.017(16)	0.023(28)
Present	1000	5000	0.090	0.165	0.001	-0.076
[27]			0.065(8)	0.102(18)	0.054(24)	-0.095(31)
Present	4000	5000	0.105	0.168	0.002	-0.065
[27]			0.180(11)	0.188(18)	0.033(19)	-0.042(28)

TABLE III: Errors in our $T\Delta S$ term encompass zero in every case. See text for details. The pressure P, temperature T, change in Gibbs free energy $\Delta G = \Delta U + P\Delta V - T\Delta S$, change in internal energy ΔU, change in volume $P\Delta V$, and change in entropy $T\Delta S$ are all calculated using MD trajectories and parameters optimized as discussed in the text. Errors are in parentheses and show the uncertainty in the digits immediately to the left.

The comparison in Table III shows decent agreement between our results for the entropy and those of Ref. [27] where thermodynamic integration was used to find the Gibb's free energy and then extract the entropy. The key comparison is the entropy value, for which we are within one sigma of the quoted value in Ref. [27] in each instance. The error in the value of the difference of the entropies in our case is hard to estimate. Each VACF integration has error associated with finite sampling [46], as in the case with deriving mass transport properties such as diffusion. In the case of a pure exponential function, the error is given by $\sqrt{2/(\gamma T_{\rm traj})}$ where γ is the inverse time constant and $T_{\rm traj}$ is the length of the integrated MD trajectory. Corrections[30] apply when the ACF is not purely exponential. In the differences that go into Table III, there are four individual error estimates to arrive at $T\Delta S$ of which the oxygen VACFs contribute the most since they have the smallest γ_2 values. However, in each case the statistical error is large enough in any one component to make the summed difference between BCC and FCC encompass zero. We cannot constrain our error bars on ΔS nearly as tightly as Ref. [27].

We note that our findings for $P\Delta V$ and ΔU are different from Ref. [27]. The main difference lies in $P\Delta V$, which we attribute to the interpolation on a finite density-temperature grid used in Ref. [27] compared to running at the same pressure in the present work. Our simulations were run to within the same pressures by 0.5%, 0.5%, and 0.2% for the (100 GPa and 3000 K), (1000 GPa and 5000 K), and (4000 GPa and 5000 K), respectively. The uncertainties in these terms are therefore expected to be much smaller than the 10%-30% found in [27].

Because the oxygen are in a solid, we numerically performed the oxygen VACF transformations to extract the solid entropy contribution (as discussed in the Al case). Fitting the functional forms in Eqs. (9) and (10) results in numerical noise due to the zero value of diffusion expected from the oxygen. The value of S is dependent on the size of the fit window due to the oscillations about zero in the tail of the oxygen VACF. Systems with pronounced phonon modes should be treated as pure solids in this method.

The lowest pressure-temperature point lies right at the BCC-FCC transition and should have the largest fluctuations. Indeed, our VACFs in the oxygen component have long time constants associated with the oscillatory behaviors which lead to a large uncertainty estimate for the entropy. It is not too surprising for our result to disagree the most here. At 1000 GPa and 5000 K we find a slightly smaller result for the entropy difference but note that statistically the results agree. At the higher pressure point but same temperature, we find a slightly smaller entropy difference but yet again within the error margin quoted in Ref. [27]. Given that only 2 MD runs are needed at each (P, T) point to establish the phases (with careful monitoring of the pressure, the pair distribution function, and energy to define the state), this can represent a vast time savings over thermodynamic integration which requires multiple runs along integration paths between the system of interest and the known system. We also note that these results, while in agreement for 54 (32) molecules in the BCC (FCC) phases, could be particle number dependent for the phase boundary, and that a study at 128 (108) molecules might reveal deviations from these values.

C. MgO

Boates and Bonev determined the metastable liquid state of MgO in their studies of $MgSiO_3$ [28]. At 10000 K and pressures between 200 GPa and 400 GPa the liquid state has higher entropy than the B1 solid state of MgO. To study the liquid state we started with a collection of 50 MgO molecules with an average molecular bond distance $r_{MgO} = 1.75\,\mathring{A}$, randomly oriented in a cubic box at a density of 5.5 g/cm^3. This was our starting configuration for the 280 GPa calculation. We let the system equilibrate using a time step of 0.75 fs, sampling at the Γ-point, and an 875 eV plane wave cut-off energy, consistent with the convergence criteria used in Ref. [28].

We could only run the 280 GPa simulation for roughly 4 ps, after a 200 fs equilibration time, because the system began to drift toward the more stable B1 solid phase. The simulation at 200 GPa used as a starting configuration a sample from the middle of the 280 GPa equilibrated run (about 1.5 ps), but with randomized initial velocities according to a Boltzmann distribution. The 240 GPa run was similarly started from an equilibrated configuration of the 200 GPa simulation.

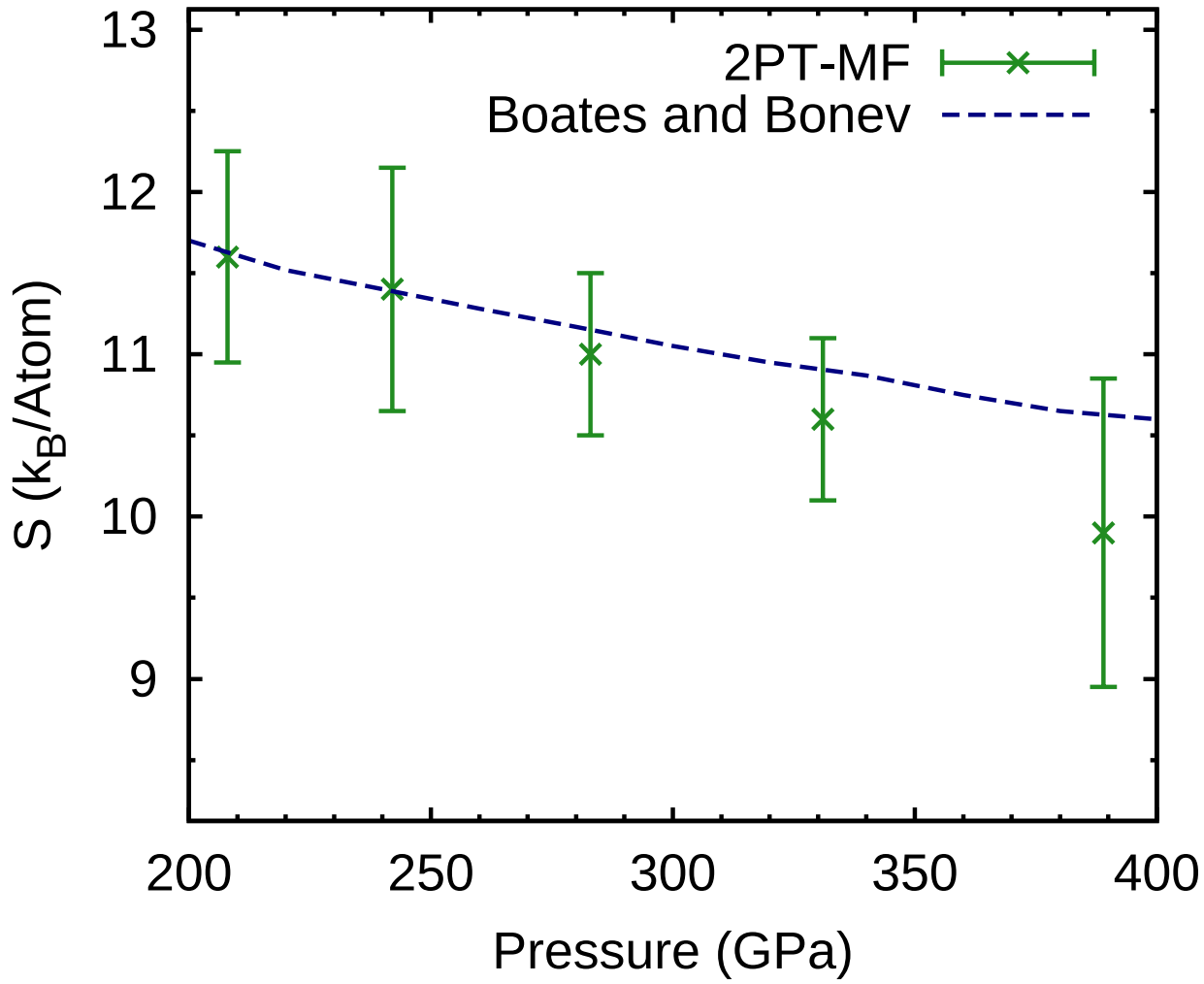

FIG. 2: (color online) Comparison of entropy vs pressure for liquid MgO with the work of Ref.[28] at 10000 K. The agreement is better than 5%. Only statistical error is considered since it is the dominant contribution to the uncertainty.

We present our results in Fig. 2 and compare with the data extracted from Figure 2d in Ref. [28]. The agreement between our method and their results is good, to within 5% save the highest pressure point. The largest limitation to improving the error is the finite trajectory due to drift to the lower B1 solid state. Therefore, we must carefully monitor the pressure and only average over the data for which the drift in the pressure/energy is minimal. In practice, we could average over a few shorter, randomized MD runs with the same pressure/energy profile to gather more statistics.

D. Al Along Ambient Isobar

As a final comparison to the method of Desjarlais[22], we compare our revised 2PT-MF method to two points, 943 K and 1200 K, along the Al ambient isobar. We ran our simulations using the Baldereshci point and an energy cut off (augmentation) of 241 (291) eV along with a 2 fs time step, consistent with the parameters of [22]. We used the volumes/atom provided by Desjarlais which produced pressures of -0.16 GPa and 0.037 GPa at 943 K and 1200 K respectively. In addition, we ran a simulation at 943 K with a smaller volume that produced a total pressure of -0.024 GPa.

At the two temperatures sampled we added the electronic portion to the entropy and found values of $S_{\rm tot} = 9.1(4)\,{\rm k_B}$/atom at T= 943 K and $S_{\rm tot} = 9.8(4)\,{\rm k_B}$/atom at T= 1200 K using the volumes provided by Desjarlais. Our smaller volume at $T = 943\,{\rm K}$ produced an entropy of $S_{\rm tot} = 8.8(4)\,{\rm k_B}$/atom, more in line with the ambient isobar value. Differences in the pressure might be due to a difference in the number of bands chosen. We used 224 (256) at 943 K (1200 K). These values are larger than found in Ref. [22], but within our quoted statistical error. As pointed out by Desjarlais [22], the 2PT method has a long tail in the frequency spectrum going as ω^{-4} and this leads to over-estimation of the entropy. Our method has a tail of order ω^{-6}, and is susceptible to the same over-estimation due to the fact that it violates the property of the third derivative (and higher order odd-derivatives) being zero at $t = 0$ for the VACF. However, because it satisfies the first derivative property, it is expected to have less over-estimation errors in the entropy values.

This also suggests routes to improve this method. First, we could take additional Padé approximants (or continued fractions) to the value of $\tilde{\mu}_0(p)$. Each succesive order gives one more odd-derivative being zero at $t = 0$ and hence tightens the ω^{-n} fall off by increasing the value of n. However, this method drastically increases the complexity and ability to analytically perform the inverse Laplace transforms of the gas and solid pieces as well as provides an increase in the number of requisite fitting parameters. Additionally, the tail in the power spectrum is not necessarily a power law and forcing higher order convergence in powers of ω^{-n} may not increase the accuracy of the entropy values obtained.

A second approach to improving the method would be to use a Gaussian for $\tilde{\mu}_0(p)$, which would preserve to all orders the odd-derivative property of the memory function at $t = 0$. However, the trade-off is the inverse Laplace transform cannot be performed analytically for $1/(p + \tilde{\mu}_0(p)$. The fits would now have to be performed in frequency space using the property

$$F(\omega) = \frac{1}{2}\left(\frac{1}{\tilde{K}(\imath\omega) + \imath\omega} + \frac{1}{\tilde{K}(-\imath\omega) - \imath\omega}\right) \tag{21}$$

where $\tilde{K}(p)$ is the total memory function including both solid and gas contributions from $\tilde{\mu}_0(p)$ and $\tilde{\mu}_1(p)$. Another advantage to this method of fitting in the frequency spectrum is there is no need to expand for small coupling parameters of the bath to the medium; we can use Eq. (1) with the Laplace transform of a Gaussian for $\tilde{\mu}_0(p)$ and the Laplace transform of a cosine for $\tilde{\mu}_1(p)$. Then after the fit, determine if λ_{01}^2 is small, and thus whether an expansion is valid for separating the VACF into gas and solid like portions, i.e. whether the gas and solid portions evolve according to their individual memory functions.

A Gaussian falls off rather quickly as a memory function, much faster than a pure exponential does. Thus, to recover the exponential behavior, but keep the even nature of $K(t)$, we can use a $sech(t/\tau)$ or $sech^2(t/\tau)$ memory function, both of which have analytic Laplace transforms. Then as done in Ref. [22], we can apply the method of moments to match the power spectrum to the coefficients in each of $\mu_0(t)$ and $\mu_1(t)$. These approaches will be explored in future work.

V. CONCLUSIONS

We have presented a method to fit the entire VACF from an MD simulation to an analytic form which separates cleanly into a gas-like and solid-like portion. These two components can then be treated as separate entities in entropic calculations and brought together in the end to provide a total entropy for the ionic contribution. This is an alteration to the 2PT-MF method [17, 18, 22] where only the gas portion was fit. We provide a model which accounts for structure in the gas and solid portions. Extending to multi-component systems is naturally contained within the fitting parameters of the model.

We've applied the model to the liquid side of the FCC Aluminum melt curve at $T = 4000\,{\rm K}$ and found good agreement to within quoted errors of the work of Robert *et al.* [23]. We also applied the model to a two-component mixture of superionic water and found decent agreement for the entropy, but mixed quality regarding the Gibb's free energies which could be traced to the $P\Delta V$ term. In the case of MgO, another two-component system, we find strong agreement in the calculation of the entropy for the metastable liquid state at 10000 K and various pressures between 200 GPa and 400 GPa.

In future work this method can be used to extract entropic information of relevance to planetary interiors[47] such as ice giants, where more complicated mixtures of methane, ammonia, and water gallivant around in myriad and complicated ways. The ability to calculate accurate entropies will be of use to planetary interior models. Additionally, complex molecular mixtures and their entropic properties are of relevance to dense plasmas in regards to inertial confinement fusion, warm dense matter, and conventional and nuclear weapons physics.

Acknowledgments

ERM is grateful for useful and inspiring discussions with Mandy Bethkenhagen and Martin French. In addition, ERM thanks Michael Desjarlais for providing his data on Aluminum for comparison. The authors gratefully acknowledge support from science campaigns 1 and 4 as well as the Advanced Simulation and Computing Program (ASC). LANL is operated by LANS, LLC for the NNSA of the U.S. DOE under Contract No. DE-AC52-06NA25396.

[1] J. D. Kirkwood, J. Chem. Phys. **3**, 300 (1935).
[2] J. A. Moriarty, D. A. Young, and M. Ross, Phys. Rev. B **30**, 578 (1984).
[3] O. Sugino and R. Car, Phys. Rev. Lett. **74**, 1823 (1995).
[4] D. Frenkel and B. Smit, *Understanding Molecular Simulation* (Academic Press, San Diego, 2002).
[5] L. Voč and D. Alfè, Phys. Rev. B **65**, 214105 (2002).
[6] J. R. Morris, C. Z. Wang, K. M. Ho, and C. T. Chan, Phys. Rev. B **49**, 3109 (1994).
[7] D. Alfè, Phys. Rev. B **68**, 064423 (2003).
[8] S. A. Bonev, E. Schwegler, T. Ogitsu, and G. Galli, Nature (London) **431**, 669 (2004).
[9] E. R. Hernández, A. Rodriguez-Prieto, A. Bergara, and D. Alfè, Phys. Rev. Lett. **104**, 185701 (2010).
[10] A. B. Belonoshko, N. V. Skorodumova, A. Rosengren, R. Ahuja, B. Johansson, L. Burakovsky, and D. L. Preston, Phys. Rev. Lett. **94**, 195701 (2005).
[11] A. B. Belonoshko, N. V. Skorodumova, A. Rosengren, and B. Johansson, Phys. Rev. B **73**, 012201 (2006).
[12] A. B. Belonoshko, S. Arapan, R. Martonak, and A. Rosengren, Phys. Rev. B **81**, 054110 (2010).
[13] J. Bouchet, F. Bottin, G. Jomard, and G. Zèrah, Phys. Rev. B **81**, 094102 (2009).
[14] A. B. Belonoshko, L. Burakovsky, S. P. Chen, B. Johansson, A. S. Mikhaylushkin, D. L. Preston, S. I. Simak, and D. C. Swift, Phys. Rev. Lett. **100**, 135701 (2008).
[15] S. N. Luo, A. Strachan, and D. C. Swift, J. Chem. Phys. **120**, 11640 (2004).
[16] K. F. Kelton, Solid State Phys. **45**, 75 (1991).
[17] S.-T. Lin, M. Blanco, and W. A. Goddard III, J. Chem. Phys. **119**, 11792 (2003).
[18] S.-T. Lin, P. K. Maiti, and W. A. Goddard III, J. Phys. Chem. B **114**, 8191 (2010).
[19] S. N. Huang, T. A. Pascal, W. A. Goddard III, P. K. Maiti, and S. T. Lin, J. Chem. Theory. Comput. **7**, 1893 (2011).
[20] P. K. Lai, C. M. Hsieh, and S. T. Lin, Phys. Chem. Chem. Phys. **14**, 15206 (2012).
[21] A. M. Teweldeberhan and S. A. Bonev, Phys. Rev. B **83**, 134120 (2011).
[22] M. P. Desjarlais, Phys. Rev. E **88**, 062145 (2013).
[23] G. Robert, P. Legrand, P. Arnault, N. Desbiens, and J. Clérouin, Phys. Rev. E **91**, 033310 (2015).
[24] I. Baraffe, G. Chabrier, and T. Barman, Rep. Prog. Phys. **73**, 016901 (2010).
[25] J. D. Lindl, P. Amendt, R. L. Berger, S. G. Glendinning, S. H. Glenzer, S. W. Haan, R. L. Kauffman, O. L. Landen, and L. J. Suter, Phys. Plasmas **11**, 339 (2004).
[26] V. F. Sears, Proc. Phys. Soc. **86**, 953 (1965).
[27] H. F. Wilson, M. L. Wong, and B. Militzer, Phys. Rev. Lett. **110**, 151102 (2013).
[28] B. Boates and S. A. Bonev, Phys. Rev. Lett. **110**, 135504 (2013).
[29] P. Damle, A. Sjölander, and K. S. Singwi, Phys. Rev. **165**, 277 (1968).
[30] E. R. Meyer, J. D. Kress, L. A. Collins, and C. Ticknor, Phys. Rev. E **90**, 043101 (2014).
[31] N. F. Carnahan and K. E. Starling, J. Chem. Phys. **53**, 600 (1970).
[32] P. H. Berens, D. H. J. Mackay, G. M. White, and K. R. Wilson, J. Chem. Phys. **29**, 2375 (1983), URL `http://dx.doi.org/10.1063/1.446044`.
[33] G. Kresse and J. Hafner, Phys. Rev. B **47**, 558 (1993).
[34] G. Kresse and J. Hafner, Phys. Rev. B **48**, 13115 (1993).
[35] G. Kresse and J. Furthmüller, Phys. Rev. B **54**, 11169 (1996).
[36] J. Hafner, J. Comput. Chem. **29**, 2044 (2008).
[37] P. Hohenberg and W. Kohn, Phys. Rev. **136**, B864 (1964).
[38] W. Kohn and L. J. Sham, Phys. Rev. **140**, A1133 (1965).
[39] N. D. Mermin, Phys. Rev. **137**, A1441 (1965).
[40] M. Weinert and J. W. Davenport, Phys. Rev. B **45**, 13709 (1992).
[41] R. M. Wentzcovitch, J. L. Martins, and P. B. Allen, Phys. Rev. B **45**, 11372 (1992).
[42] G. Kresse and J. Firthmuller, Comp. Mat. Sci. **6**, 15 (1996).
[43] P. E. Blöchl, Phys. Rev. B **50**, 17953 (1994).
[44] G. Kresse and D. Joubert, Phys. Rev. B **59**, 1758 (1999).
[45] J. P. Perdew, K. Burke, and M. Ernzerhof, Phys. Rev. Lett. **77**, 3865 (1996).
[46] M. P. Allen and D. J. Tildesley, *Computer Simulation of Liquids* (Oxford University Press, USA, 1989), ISBN 0198556454.
[47] E. R. Meyer, C. Ticknor, M. Bethkenhagen, S. Hamel, R. Redmer, J. D. Kress, and L. A. Collins, The Journal of Chemical Physics **143**, 164513 (2015).